Appl Phys B (2011) 104:481–486
DOI 10.1007/s00340-011-4635-8

Applied Physics B
Lasers and Optics

Fiber waveguide arrays as model system for discrete optics

U. Röpke · H. Bartelt · S. Unger · K. Schuster · J. Kobelke

Received: 8 April 2011 / Revised version: 9 May 2011 / Published online: 9 July 2011

Abstract Optical waveguide arrays consisting of a two-dimensional arrangement of weakly coupled waveguides represent the basis of the new research field of discrete optics. For studying the nonlinear pulse dynamics, fiber waveguide arrays offer specific advantages such as a high optical damage threshold and an accessible range of anomalous dispersion. Coherent coupling of such waveguides for reasonable propagation lengths requires, however, a high structural quality of the waveguides and their superstructure, which is beyond conventional fiber technology. Design, fabrication and characterization of such a fiber waveguide array are described. The linear propagation properties in such a system are modeled and compared with experimental measurements. The high structural homogeneity and good optical quality of the arrays as well as the limits of the nearest-neighbor approximation are demonstrated.

1 Introduction

Evanescently coupled optical waveguides present a wide field of research, which has been investigated for many years in 1D (one-dimensional, planar) and 2D configurations. In particular, the interest in multicore fibers is motivated by signal processing (e.g. couplers, splitters, combiners, filters, nonlinear switches) by means of passive cores and by the development of high power fiber lasers using laser-active cores. Apart from an assembly of conventional waveguides, multicore photonic crystal structures have been applied to extend the capabilities of fiber optics.

U. Röpke · H. Bartelt (✉) · S. Unger · K. Schuster · J. Kobelke
Institute of Photonic Technology, Albert-Einstein-Str 9,
07745 Jena, Germany
e-mail: hartmut.bartelt@ipht-jena.de

In recent years there has been an increasing interest in the use of multicore fibers in the context of artificial optical media, especially in discrete optical materials [1]. Such materials are composed of weakly coupled waveguides, which are arranged in a periodic structure (2D waveguide arrays). Therefore, the spatial degrees of freedom of the optical field are reduced in the transversal directions from continuous to discrete values. The diffraction in this material can be controlled by the coupling strength of the waveguides ("discrete diffraction"). The related optics, which is referred to as "discrete optics", exhibits unique propagation properties which differ strongly from light field evolution in continuous media. Besides phenomena of linear optics (e.g. [2–4]) also the interplay of discrete diffraction, dispersion und nonlinear effects has attracted great interest [5].

Experimental investigation in this field was made possible by the implementation of 2D discrete media during the last decade. The fabrication techniques include optical induction of lattices in photorefractive materials [6], femtosecond laser writing of waveguide arrays [7, 8], and fiber-optical technology applied to multicore fibers [3, 9, 10]. Most experimental results were obtained using the first two fabrication methods. However, until recently the theoretically predicted spatio-temporal solitons (3D-light bullets) [11, 12], which are a unique feature of discrete optics, could not be proven experimentally because of the absence of a suitable model system of a discrete medium. Fiber-optic waveguide arrays appeared to be especially promising because of, for instance, their guiding properties in the spectral range of anomalous dispersion of silica (1.55 μm) and their high optical damage threshold. We succeeded in solving the problem of disorder in array fibers [10], following new concepts in the fabrication of high-precision array fibers [1].

Using this concept, we will discuss in the following section hexagonal waveguide array fibers with 91 cores,

in which 3D-light bullets have been observed successfully [12]. Design, fabrication, application characteristics, modeling considerations and the structural quality of the resulting arrays are discussed. In the third section, the optical properties of the arrays are investigated from two viewpoints: the influence of residual disorder on the coherent coupling mechanism on the one hand, and the significance of other coupling mechanisms except nearest-neighbor coupling on the other. To this end, a measurement method is proposed and applied which determines the propagation properties of light at a fixed array length by wavelength scanning.

2 Fiber array waveguide design and fabrication method

2.1 General design and technology requirements

Experimental investigations of nonlinear pulse dynamics in discrete optics make specific parameter adjustments in the waveguide array structure necessary. The study of the interplay of waveguide coupling (discrete diffraction), nonlinear effects and pulse dispersion requires comparable strengths of these mechanisms [1, 12]. Therefore, the array should be characterized by a high material damage threshold and a weak coupling of the waveguides. As a waveguide coupling parameter we use the propagation length L_C (coupling length) of total power exchange between two adjacent waveguides (note that six adjacent waveguides result in a power exchange length $L_C/\sqrt{6}$) [13]. The aim is to achieve $L_C > 50$ mm (see detailed discussion in [1]). In order to maintain a coherent coupling at such propagation lengths, the variations of the effective index Δn_{eff} of the fundamental waveguide modes should be kept well below 10^{-5} (resonant waveguides), which represents a high technological challenge. Similarly, in order to achieve homogeneous array coupling, the variations of L_C should be kept small, which implies an extremely regular hexagonal array structure (including the array boundary). The challenging requirements are met by suitable selection of the raw materials, the specific structural design and a careful fabrication process.

Fiber-optic waveguide arrays are special microstructured fibers, which can be fabricated by the well-established technology of composite preforms. For the intended high-quality fiber-optical waveguide arrays, in a first step the waveguiding and buffer elements are prepared separately. In a second step these elements are packed according to the design structure and mounted in an evacuable jacketing tube. The resulting composite preform is consolidated in a last step within a fiber drawing furnace and then drawn into the waveguide array fiber. The outer diameter of the produced fiber is closely related to the structural array parameters. Therefore, a set of experimentally interesting array fibers can be obtained from a single composite preform by varying the outer diameter of the fiber in the drawing process.

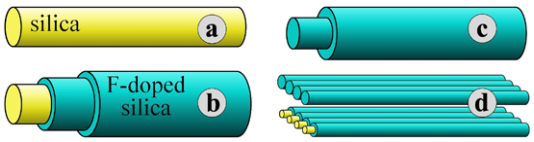

Fig. 1 Preparation of the waveguiding and buffer elements of the composite preform: (**a**) cylindrical high-purity silica rod; (**b**) preform for waveguiding elements with F-doped silica as cladding material; (**c**) preform for buffer elements made from F-doped silica; (**d**) final elements for the composite preform

2.2 Specific design and fabrication of preform elements

The waveguiding elements of the composite preform were prepared by the rod-in-tube technique. As a core, a closely toleranced cylindrical rod from high-purity silica (Heraeus F300, diameter 12 mm ±0.1%, Fig. 1a) was used. It was double-jacketed with fluorine-doped silica tubes (Heraeus F320) as a cladding material and ultrasonically ground in order to tune the core-cladding ratio and to improve the cylindricity and concentricity of the resulting preform of the waveguiding elements (Fig. 1b). In the same way, but without the core material and the grinding process step, a preform of the buffer elements was prepared (Fig. 1c). Finally, the preform elements were elongated within a close tolerance to obtain the final elements of the composite preform (diameter 1.4 mm ±0.1%, Fig. 1d).

The materials were selected so as to fulfill the high demands required for use of the array fibers in discrete optics. The silica core material is characterized by high optical homogeneity and good optical power stability. The F-doped cladding material shows some limited refractive index gradients due to heat-induced out-diffusion of fluorine in the fabrication processes, which is less critical in the region of the evanescent fields and for the intended infrared region. The small inhomogeneities can be observed by means of microscopic techniques and can be used to investigate the structural quality of the array as demonstrated below in Fig. 3c.

An important feature of the selected materials is the small index difference $\Delta n = 1.2 \times 10^{-3}$ between the core and cladding materials, which allows a large-mode-area design, e.g. a core radius $r = 9.5$ µm and a cutoff wavelength $\lambda_{\text{cutoff}} = 1.46$ µm (waveguide parameter $V = 2.405$ [13]). Due to the large structural dimensions and the low numerical aperture (NA = 0.06), the influence of point-like material inhomogeneities (e.g. at the interfaces between the elements) and the requirements on the optical components for excitation and detection of array light are less critical. Furthermore, the viscosity difference of the materials used has a markedly favorable effect on the structural change during the consolidation process of the composite preform elements. The higher viscosity of the cores preserves their circular shape, while the low-viscosity cladding material fills the gaps between the preform elements and thereby reduces

the core distance (pitch Λ) by a factor of 0.9523. Finally, the specific structural design with circular cores and an almost step-index profile supports the simplicity of light propagation modeling, e.g. by the weak guidance ($\Delta n \ll 1$, scalar theory) or by weak coupling ($\lambda/\Lambda \ll 1$, coupled-mode theory). The specific array structure and basic parameters are shown in Fig. 2a.

A design value of the pitch $\Lambda = 34$ µm was obtained from the theory of two coupled waveguides [13] using the core parameters r and Δn as given above, the wavelength $\lambda =$ 1550 nm and the intended coupling length $L_C = 57$ mm. From these parameters, the core-cladding ratio of the waveguiding elements, 1.905 $r/\Lambda = 0.532$, is obtained.

2.3 Buffer region and jacketing

In order to achieve high-quality waveguide arrays with good application characteristics, a surrounding buffer region and the transition to the jacketing tube must be suitably designed. As a second function, the buffer region improves the application characteristics of the array. It prevents guided light from interacting with the surrounding area. In addition, background radiation, caused e.g. by the excitation of the array, is dispersed and can be attenuated at the outer diameter of the array fiber, e.g. by index gel.

A hexagonal package of preform elements fits badly with a circular jacketing tube. This does cause significant deviations from a regular array during the consolidation process. In order to balance the structural differences, the waveguide array was surrounded by a buffer region consisting of buffer elements. An irreducible 30° sector of the fabricated structure is shown in Fig. 2b. The inner region of the jacketing tube (high-purity silica, Heraeus F300) includes the hexagonal package of waveguiding and buffer elements and, additionally, 3 types of special buffer elements for good transition to the cylindrical geometry. The diameters of these elements were chosen to be 100%, 94.2% and 74%, respectively, of the standard diameter in order to minimize azimuthal material transport during the consolidation process. Figure 3a shows the composite preform (made up of 253 elements) and the jacketing tube. A cross-section of a drawn array fiber with outer diameter 681 µm is demonstrated in Fig. 3b. The array consists of 91 circular cores with $\Delta n = 1.2 \times 10^{-3}, r = 9.7$ µm, and $\Lambda = 34.8$ µm. The border lines between the elements are visualized in Fig. 3c. A regular honeycomb pattern and a small transition region to the circular jacketing demonstrate the high quality of the array geometry including the array boundary. Variations of the core distances are smaller than the resolution limit of 0.5 µm of the microscopical analysis. Consequently, the coupling strength between the cores is nearly constant. For experimental investigations, additional fiber diameters of 470 µm ($r = 6.7$ µm, $\Lambda = 24$ µm), 580 µm ($r = 8.25$ µm, $\Lambda = 29.6$ µm) and 818 µm ($r = 11.65$ µm, $\Lambda = 41.8$ µm) were also drawn.

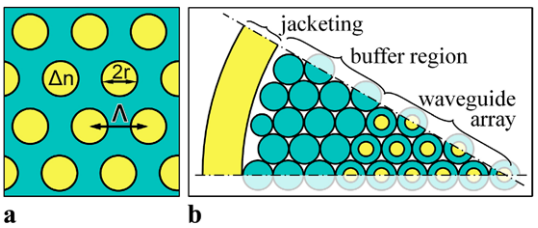

Fig. 2 (**a**) Sketch of the array structure and basic array parameters; (**b**) overall structural design of the composite preform (irreducible 30° sector of the hexagonal structure)

3 Investigation of linear optical propagation properties

The investigation of the linear propagation properties of light in the fiber array waveguides is intended to give insight into two different questions, viz. the optical quality achieved in the fabricated array, and the physical functionality of the waveguide array, the latter by comparing experimental results with modeling of light propagation using the well-established first-order nearest-neighbor approximation. The first question is connected with random deviations from the ideal array, especially considering the optical phase mismatch of the waveguides. The second question refers to the actual complexity of array coupling in view of the weak coupling design of the arrays and the commonly used model.

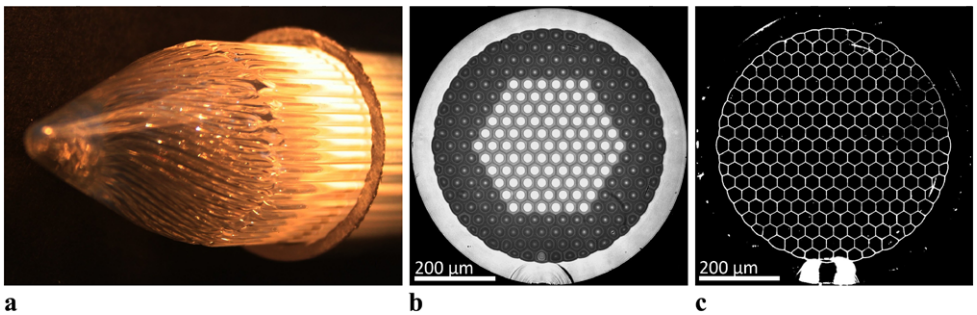

Fig. 3 (**a**) Composite preform (end section and jacketing tube); (**b**) cross-section of an array fiber with 91 cores and 681 µm outer diameter (white light transmission microscopy); (**c**) structure of element border lines (dark-field reflected-light microscopy of a cleaved and etched facet)

3.1 Applied model of light propagation

Finite waveguide arrays are complex optical multimode systems. The complexity of the description can be reduced by using special array characteristics as a basis for an approximative approach. The weak coupling approximation takes advantage of the exponentially decreasing evanescent fields of the waveguides. In zeroth order the array consists of isolated, equidistant (circular shape, step-index profile, weakly guiding) waveguides. The light is represented by the constant complex-valued field amplitudes u_i $(i = 1, \ldots, 91)$, which will be summarized in a vector $u = \{u_i\}$ and are set by suitable excitation at the input facet. Experimentally accessible at the output facet is the relative power p_i:

$$p_i = |u_i|^2 / \sum_k |u_k|^2. \tag{1}$$

The first-order approximation takes into account the coupling of nearest neighbors. Here, the coupling length L_C expresses the strength, and the coupling matrix M_C represents the neighborhood relations ($M_{C;ik} = 1$ if i, k refer to adjacent cores, otherwise $M_{C;ik} = 0$). In this approximation, the coupled-mode theory results in the propagation equation (vector form) [1]:

$$\frac{du(\varsigma)}{d\varsigma} = i\frac{\pi}{2} M_C u(\varsigma). \tag{2}$$

Here, the propagation length z and the coupling length L_C are represented by the propagation parameter $\zeta = z/L_C$. Now the field amplitudes u_i are functions of ζ. Using the input vector $u(0)$ and an array sample length L, the amplitude vector $u(\zeta_L)$ at the output facet follows from (2):

$$u(\varsigma_L) = \exp\left(i\frac{\pi}{2}\varsigma_L M_C\right) \cdot u(0), \tag{3}$$

where a matrix exponential function of the propagation parameter $\zeta_L = L/L_C$ of the sample is combined with the input vector by a scalar multiplication.

The coupling length L_C is a function of the wavelength λ and the array parameters Λ, r and Δn, and can be obtained from the theory of two coupled waveguides [1, 13]. Using a sample length of $L = 55$ mm and considering that the ratio r/Λ is fixed for different array fiber diameters, $\zeta_L(\lambda, \Lambda)$ was calculated as shown in Fig. 4 by solid lines.

3.2 Experimental measurement method

In our experimental approach for characterizing the properties of the fiber waveguide array, we scanned the transmitted wavelength over a wide range of wavelengths. In this way, the propagation parameter ζ_L is directly varied, and the need for using a large assortment of samples with different

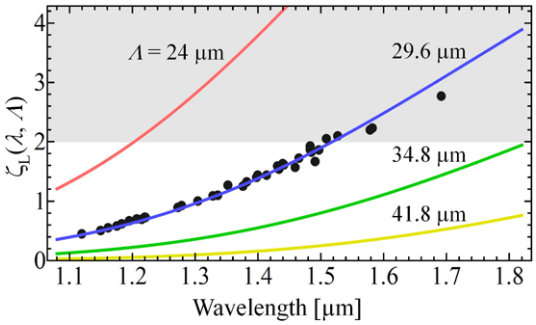

Fig. 4 Propagation parameter ζ_L as a function of the wavelength λ and array pitch Λ with sample length $L = 55$ mm; *lines*: calculated data using the theory of two adjacent waveguides; *points*: coordinates (λ, ζ_L) mark nearly identical patterns obtained from experimental measurements at wavelength λ, $\Lambda = 29.6$ µm, and by modeling at ζ_L. In the *shaded range* ($L_C < 27.5$ mm), discrepancies between experiment and modeling are observed

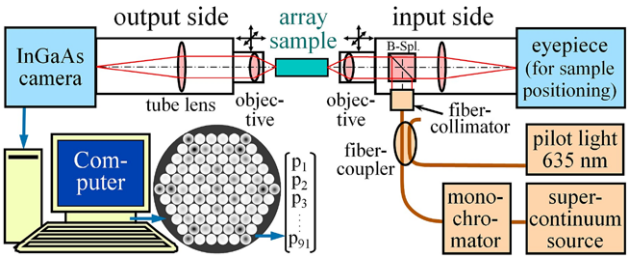

Fig. 5 Set-up for the wavelength scanning measurement method

lengths is avoided. In this case the measuring set-up must be designed for a broad spectral range, but the free access to a parameter of central significance is of great value. Figure 5 shows the scheme of the set-up.

The light from a supercontinuum source (Fianium SC400) and a monochromator (Oriel 77250) is coupled into a standard single mode fiber (SMF-28). At the input side of the sample, a light beam is generated, which selectively excites the fundamental mode of a single waveguide core. In this case all but one component of the input field vector $u(0)$ in (3) become zero. To focus and position the beam, the optical components (objective 10× Mitutoyo NIR with NA 0.26, beam splitter, fiber collimator and tube lens) were mounted on a 3-axis micropositioner. A similar configuration was used on the output side. The magnified image of the output facet is captured by an infrared camera (Indigo Alpha NIR, 320×256 pixel) and processed by a computer to obtain images of the intensity distributions and the relative power p_i of different waveguide cores at the output facet. The position of the focus on the input facet can be controlled by a pilot light and an eyepiece. Higher-order modes were suppressed by carefully adjusting the excitation point and applying index gel at the array jacketing. Moreover, to prevent coherent noise, the incident beam had a spectral width

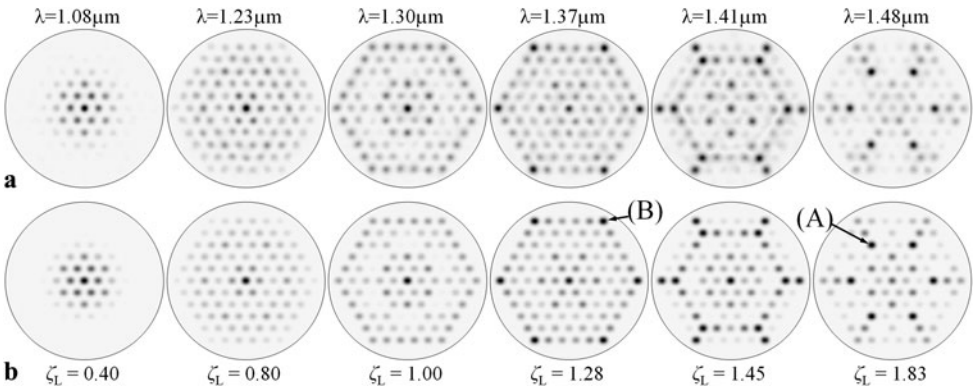

Fig. 6 Intensity distribution patterns of the array ($L = 55$ mm, $\Lambda = 29.6$ μm, inverted normalized representation, central excitation): (**a**) experimental patterns as a function of the wavelength λ; (**b**) equivalent patterns obtained from the model calculations with a best fit value of ζ_L. The labels (*A*) and (*B*) mark groups of cores at symmetrically equivalent positions, which are referred to in Fig. 7 as type (*A*) and type (*B*) cores

of 20 nm. The scanning range of the wavelength was 1.08–1.84 μm.

The lines in Fig. 4 can be used as $\zeta_L - \lambda$-characteristic curves. From a sample length of $L = 55$ mm and a pitch of $\Lambda = 29.6$ μm (array fiber diameter 580 μm, $\lambda_{\text{cutoff}} = 1.27$ μm), a propagation parameter range from $\zeta_L = 0.4$ to $\zeta_L = 4$ is obtained. With $\Lambda = 34.8$ μm (diameter 681 μm), the upper limit of ζ_L is reduced by half. It can be recompensated for by doubling the sample length, which doubles the values of the ζ_L-axis. (Note that in this case the phase mismatch between the waveguide modes is also doubled.)

4 Results and discussion

There are many interesting measurement conditions possible using different excitation points, pitch values and sample lengths. In view of the large amounts of data to be analyzed and the application of the array fibers in experiments on 3D-light bullets [12], the results discussed here are restricted to the case of a centrally excited array with sample length $L = 55$ mm and pitch $\Lambda = 29.6$ μm. Distinctive output patterns at certain wavelengths were related to calculated patterns by visual comparison. Up to a wavelength of 1.52 μm, both experiment and model are well correlated, and matching values of ζ_L were found with an uncertainty of ± 0.1. The results are plotted as points in Fig. 4. From the good agreement with the corresponding line obtained from the theory of two coupled waveguides, we conclude that for $\lambda < 1.52$ μm, $\zeta_L < 2$ the coupled-mode theory with nearest-neighbor approximation describes the light propagation quite well. Some specific examples are shown in Fig. 6. Random deviations from symmetry are small in all cases.

At wavelengths $\lambda > 1.52$ μm, correlation with the model deteriorates and sometimes fails due to random and systematic deviations. To distinguish between disordering effects and symmetry-maintaining mechanisms, symmetrically equivalent core positions were grouped together and compared with each other and the model results. Examples

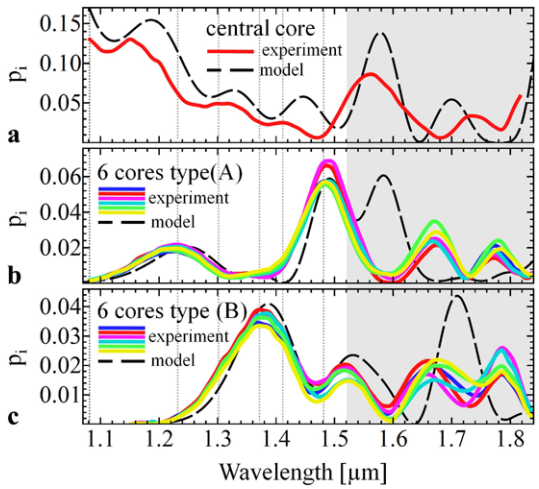

Fig. 7 Relative output power p_i as a function of λ for selected symmetrically equivalent cores (centrally excited array, $L = 55$ mm, $\Lambda = 29.6$ μm): (**a**) central core of the array, (**b**) and (**c**) 6 cores at equivalent positions (*A*) and (*B*), respectively. The wavelengths marked by *dotted lines* and the cores of type (*A*), (*B*) refer to Fig. 6. In the *shaded range*, discrepancies between experiment and modeling occur

are given in Fig. 7, which shows the relative power as a function of λ for the central core and for two groups labeled in Fig. 6 by (A) and (B). Here again, the random deviations of the measured curves are moderate. Obviously there are discrepancies between experiment and model for wavelengths beyond 1.52 μm, which cannot be attributed to random irregularities of the array. Rather they reflect a more complex coupling of the waveguides than supposed in the nearest-neighbor-approximation model.

The discrepancies between experiment and modeling are found at longer wavelengths, where the coupling strengths of different approximation orders approach each other. As an example, the ratio of the next-nearest and nearest-neighbor coupling strengths increases from 1:430 at $\lambda = 1.08$ μm to 1:38 at 1.52 μm and 1:13 at 1.84 μm. At longer wavelengths, higher-order effects may possibly alter the sensitive mechanism of coherent coupling. Therefore, an im-

proved model should take into account the strongest second-order effects. Candidates are the second-order coupling of nearest neighbors, the first-order coupling of next-nearest neighbors, and effects caused by the non-orthogonality of the coupled modes. To our knowledge, up to now such an involved analysis has been carried out only for one-dimensional arrays [14, 15].

However, the experiments indicate a limit for the applicability of the model (3) at $L_C = 27.5$ mm. In Fig. 7 and Fig. 4 the range of inconsistency is shaded. As shown in Fig. 4, the model is applicable throughout the spectral range if an array pitch $\Lambda = 34.8$ µm (fiber diameter 681 µm) is selected, as in the study of 3D-light bullets [12]. The suitability of the nearest-neighbor-approximation model in this case was also directly confirmed by experiment.

5 Conclusion

We have demonstrated the design and preparation of high-quality fiber waveguide arrays having good application properties for the investigation of discrete optical propagation effects. The ensurance of low refractive and geometrical inhomogeneities at levels well beyond conventional fiber technology represents a major technological challenge. A wavelength scanning measurement method for the optical characterization of arrays has been proposed and applied. The comparison of model calculations on the basis of the commonly used nearest-neighbor approximation and experimental investigations shows good agreement for coupling lengths greater than 27.5 mm (array length 55 mm). The well-defined propagation properties in this range have been the basis for the successful demonstration of light bullet propagation in such waveguide arrays [12]. It has also been shown that for shorter coupling lengths the nearest-neighbor approximation is no longer suitable and additional effects have to be included in the propagation model.

Acknowledgements This work was funded by the DFG within research unit 532 "Nonlinear Dynamics". Fruitful cooperations and discussions with the partners in the research unit are gratefully acknowledged.

References

1. U. Röpke, H. Bartelt, S. Unger, K. Schuster, J. Kobelke, Opt. Express **15**, 6894 (2007)
2. E. Suran, F. Louradour, A. Barthélémy, A. Kudlinski, G. Martinelli, Y. Quiquempois, M. Douay, Opt. Lett. **34**, 2536 (2009)
3. A. Szameit, T. Pertsch, F. Dreisow, S. Nolte, A. Tünnermann, U. Peschel, F. Lederer, Phys. Rev. A **75**, 053814 (2007)
4. A. Szameit, I.L. Garanovich, M. Heinrich, A.A. Sukhorukov, F. Dreisow, T. Pertsch, S. Nolte, A. Tunnermann, S. Longhi, Yu.S. Kivshar, Phys. Rev. Lett. **104**, 223903 (2010)
5. J. Fleischer, G. Bartal, O. Cohen, T. Schwartz, O. Manela, B. Freedman, M. Segev, H. Buljan, N. Efremidis, Opt. Express **13**, 1780 (2005)
6. N. Efremidis, S. Sears, D. Christodoulides, J. Fleischer, M. Segev, Phys. Rev. E **66**, 046602 (2002)
7. S. Nolte, M. Will, J. Burghoff, A. Tuennermann, Appl. Phys. A, Mater. Sci. Process. **77**, 109 (2003)
8. A. Szameit, D. Bloemer, J. Burghoff, T. Pertsch, S. Nolte, F. Lederer, A. Tuennermann, Appl. Phys. B **82**, 507 (2006)
9. T. Pertsch, U. Peschel, J. Kobelke, K. Schuster, H. Bartelt, S. Nolte, A. Tunnermann, F. Lederer, Phys. Rev. Lett. **93**, 053901 (2004)
10. T. Pertsch, A. Chipouline, S. Nolte, F. Lederer, U. Röpke, J. Kobelke, K. Schuster, H. Bartelt, U. Peschel, A. Tünnermann, in *Photonic Metamaterials: From Random to Periodic* (Optical Society of America, Washington, 2006), paper WA7,
11. Y. Silberberg, Opt. Lett. **15**, 1282 (1990)
12. S. Minardi, F. Eilenberger, Y.V. Kartashov, A. Szameit, U. Röpke, J. Kobelke, K. Schuster, H. Bartelt, S. Nolte, L. Torner, F. Lederer, A. Tünnermann, T. Pertsch, Phys. Rev. Lett. **105**, 263901 (2010)
13. A.W. Snyder, J.D. Love, *Optical Waveguide Theory* (Chapman & Hall, London, 1983) p. 387 et seqq, p. 567 et seqq
14. M.L. Cooper, S. Mookherjea, Opt. Express **17**, 1583 (2009)
15. C. Minot, N. Belabas, J.A. Levenson, J.-M. Moison, Opt. Express **18**, 7157 (2010)